# Spectral signatures of critical charge and spin fluctuations in cuprates

M. Grilli [a], S. Caprara [a], C. Di Castro [a], T. Enss [b], R. Hackl [c], B. Muschler [c], and W. Prestel [c]

[a] *Dipartimento di Fisica, Università di Roma "Sapienza' e SMC-IMFM-CNR, P.le A. Moro, 00185 Roma, Italy*
[b] *Technische Universität München, Physik Department T34, James-Franck-Str., D-85747 Garching, Germany*
[c] *Walther-Meissner-Institut, Bayerische Akademie der Wissenschaften, Walther-Meissner-Strasse 8, 86748 Garching, Germany*

**Abstract**

We discuss how Raman spectra of high temperature superconducting cuprates are affected by nearly-critical spin and charge collective modes, which are coupled to charge carriers near a stripe quantum critical point. We find that specific fingerprints of nearly-critical collective modes can be observed and that the selectivity of Raman spectroscopy in momentum space may be exploited to distinguish the spin and charge contribution. We apply our results to discuss the spectra of high-$T_c$c superconducting cuprates finding that the collective modes should have masses with substantial temperature dependence in agreement with their nearly critical character. Moreover spin modes have larger masses and are more diffusive than charge modes indicating that in stripes the charge is nearly ordered, while spin modes are strongly overdamped and fluctuating with high frequency.

*Key words:* Quantum criticality, stripes, Raman spectra
*PACS:*

## 1. Introduction: The anomalous phase vs quantum criticality debate

The origin of the anomalous metallic behavior of the superconducting cuprates is still debated. One possibility is that the strongly correlated nature of these doped Mott insulators, together with their nearly two-dimensional electronic structure, gives rise to a stable metallic phase with non-Fermi-liquid (non-FL) properties. Since the early days of high- $T_c$ superconductivity the proposal of a resonating valence bond (RVB) state [1] was put forward with properties similar to those of the Luttinger liquid in one-dimensional systems [2]. Another proposal for a non-FL phase is related to the formation of nearly one-dimensional striped textures in the underdoped cuprates [3]. In this case the non-FL properties are structurally inherent to the strongly inhomogenous electronic liquid state. In both cases, the non-FL character of the cuprates is an intrinsic property of the ground state "*per se*".

A completely different point of view relates the anomalous properties to the proximity to some second-order phase transition. In this case abundant long-range fluctuations of the order parameter can couple to the electrons strongly affecting their properties. In particular, the instability line may extend to zero temperature by increasing doping ending into a quantum critical point (QCP) [5,6,7]. Thus the fluctuations acquire the dynamical character of collective modes (CMs), which couple to the electrons mediating a *retarded* effective interaction. Owing to their nearly critical character, these CMs have low typical energy scales and retardation plays a relevant role. Anomalous properties then naturally arise from the strong dynamical fluctuations. The two above alternative points of view (namely the non-FL phase and the QCP scenario) precisely find a counterpart in the different nature of effective interactions: While in the non-FL phase the interactions may well be instantaneous (like, e.g., a magnetic coupling J forming the singlet spin liquid in the RVB phase), the QCP scenario relies on the presence of low-energy modes mediating retarded interactions. These interactions also mediate pairing giving rise to the so-called "glue" issue: understanding the retarded or non-retarded character of pairing would shed light on the whole physics of the cuprates. This explains the growing interest in the "glue" issue both from the theoretical [4,8] and experimental [9,10] side.

## 2. The CO-QCP scenario

The presence of non-FL behavior close to QCP's in different correlated systems like the heavy fermions indirectly supports to the relevance of this scenario for the cuprates. Yet the QCP line of reasoning allows for a variety of pos-

sible realizations. One possibility is that the instability is (nearly) local in space and the instability gives rise to a (nearly) local QCP, with the destruction of the FL state being induced by the formation of local singlets [11]. In this case the critical fluctuations are expected to be rather structureless in momentum space. On the other hand, strongly peaked fluctuations at zero momentum are expected if the system becomes unstable because of the formation of a spatially uniform state like in the case of a Pomeranchuk instability [12] or of a circulating current state breaking time reversal symmetry[5]. The formation of a state breaking translational invariance naturally leads to fluctuations strongly peaked at momenta related to the wavelength of the ordered state. This is the case of the antiferromagnetic (AF) state, with a transition accompanied by critical spin fluctuations strongly peaked at $\mathbf{Q}_s \approx (\pm\pi, \pm\pi)$. The AF state occurs in cuprates at very low doping and rapidly dies upon hole doping. Thus, disregarding disorder effects, possibly leading to glassy phases at low temperature, one expects the QCP to be located at low doping and the related physical effects (pseudogap, superconductivity, magnetic and transport properties, and so on) to emanate at moderate-to-optimal doping starting from this low-doping QCP [7].

Here we discuss evidences indicating that the physics of cuprates is affected by the proximity to a charge-ordering (CO) QCP located near optimal doping [13]. The CO-QCP merges two relevant issues in the cuprates: the issue of charge inhomogeneities and of quantum criticality. The first one arose theoretically from the finding of striped phases in mean-field treatments of the Hubbard model [14]. Striped phases (as well as other inhomogeneous phases) can also be found when the tendency to phase separation, common for strongly correlated systems is frustrated by the long-range Coulomb force preventing segregation of charged carriers [3,15,16]. Following this latter approach to stripes, the CO instability was first analyzed in Ref. [6] in the framework of quantum criticality. While in real systems true long-range charge order is prevented by the competing formation of pairs, by disorder, and by the two-dimensional structure of the copper-oxide planes, the physical properties of cuprates are strongly affected by low-energy charge fluctuations on large domains. The putative instability line would end in a QCP around optimal doping. In this framework the overdoped region corresponds to the quantum disordered side of the phase diagram, the optimally doped region corresponds to the quantum critical and the underdoped region corresponds to the nearly ordered region. It is worth remarking that this "missed" QCP is not alternative to the presence of strong spin fluctuations due to the AF state at low doping. On the contrary, the intrinsically inhomogeneous CO state creates regions with lower hole density, where spin degrees of freedom are important. Therefore charge fluctuations due naturally "enslave" spin fluctuations and bring the relevance of these degrees of freedom up to substantial dopings. This may account for the presence of sizable spin excitations observed by inelastic neutron scattering up to large doping levels in $La_{2-x}Sr_xCuO_4$ (LSCO) compounds [22,23,24,25].

The CO-QCP scenario was then extendend by relating the CO-QCP with d-wave superconductivity and the pseudogap formation [17] and with their isotopic dependencies [18]. The effects of critical CO fluctuations on ARPES [19], optical [20] and Raman [21] spectra were subsequently explored.

We will show here that Raman spectra in LSCO are consistent with the simultaneous presence of nearly-critical charge and spin fluctuations, these latter displaying properties in agreement with the spectra observed by neutron experiments.

## 3. The spin and charge collective modes

The charge- and "enslaved" spin-fluctuation propagators near the CO-QCP has the generic form prediceted by the Hertz [26] theory of quantum criticality with dynamical critical exponent $z = 2$

$$D_\alpha(\mathbf{q}, \omega_n) = -\frac{g_\alpha^2}{m_\alpha + \nu_\alpha(\mathbf{q} - \mathbf{q}_{\alpha c})^2 + |\omega_n| + \omega_n^2/\overline{\Omega}_\alpha} \qquad (1)$$

where $\alpha = c, s$ refers to charge or spin fluctuations. The same form of the charge CM (but for the $\omega^2$ term in the denominator) was microscopically calculated within a strongly-correlated Hubbard-Holstein model in Ref. [6], where the presence of a QCP around optimal doping was first predicted using realistic parameters for the cuprates. For spin modes, Eq. (1) has been customarily considered in theories involving spin fluctuations [7]. Here, $\omega_n$ are boson Matsubara frequencies, $g$ is the QP-CM coupling, $\nu$ is a fermion scale setting the rapid increase of the denominator when the CM momenta move away from the critical ones. This dispersive term is assumed to have an intrinsic cutoff $\Lambda$ above which the CM no longer exists. $m_c \propto \xi^{-2}$ is proportional to the inverse square correlation length and it measures the distance to the CO transition. The mass $m_s$ of the "enslaved" spin CMs can follow the charge CM mass, but no theory has yet been elaborated for this effect and in the following it will be phenomenologically determined. In a recent work [27] we pointed out that the subleading $\omega^2$ term not only arises from higher-order contributions of the electronic particle-hole excitations, but, in the case of charge modes, it relates fermions and phonon scales and encodes the dynamical nature of the phonons thereby introducing the cutoff $\overline{\Omega}_c$. Typical values were estimated to range from tens to several hundreds of $cm^{-1}$ [27]. For spin fluctuations, a similar term arises from the coupling to higher-energy propagating spin modes yielding a somewhat larger scale $\overline{\Omega}_s$ of the order of thousends of $cm^{-1}$. While these terms play a relevant role in optical conductivity by setting the momentum-dissipation scale [27], here we point out a different physical role by individually discussing the role of the different terms in the denominator of Eq. (1). The mass $m$ represents the mini-

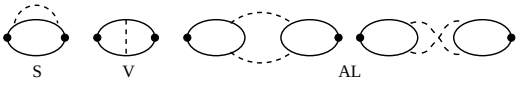


Fig. 1. Diagrams for the CM corrections to the optical or Raman response function. The full dots represent the current or Raman vertices. The solid lines represent the QP propagator and the dashed lines represent the interaction mediated by CO or AF CM. Self-energy, vertex, and Aslamazov-Larkin-like contributions are labeled by S, V, and AL, respectively.

mal energy required to create a fluctuation peaked around momenta $\mathbf{q}_\alpha$, while the linear frequency term extablishes the diffusive (i.e. relaxational) character of these fluctuations arising from the damping due to decay into particle-hole pairs. The $\omega^2$ term, once it is analitically continued to real frequencies, sets the propagating character of the CM above the $\overline{\Omega}$ energy. The propagation then follows the $\sqrt{\overline{\Omega}(m+\nu(\mathbf{q}-\mathbf{q}_\alpha)^2)}$ dispersion. Were it not for the diffusive part of the CM spectrum, the propagating part would then occur in the range between $\omega_1 \approx \sqrt{\overline{\Omega} m}$ and $\omega_2 \approx \sqrt{\overline{\Omega}\Lambda}$. In this case the spectral distribution of the modes closely resembles the "gapped marginal-FL" one considered in Ref. [28] to describe optical conductivity. The main advantage of the present form is that Eq. (1) describes both a diffusive low-energy regime important for the leading critical behavior and propagating behavior at intermediate-high energies relevant in Raman and optical spectra. Moreover, the link between Eq. (1) and specific microscopic models allows for estimates of the relevant parameters and for a transparent interpretations of the physically relevant absorption mechanisms.

In the following we will mostly focus on the Raman spectra to identify from symmetry arguments the role of spin and charge fluctuations in the various Raman channels. In this framework we will consider different processes reported in Fig. 1 The S-V terms represent the perturbative "dressing" of the QPs by the CMs. On the other hand, the AL diagrams closely resemble those of the Aslamazov-Larkin theory of paraconductivity due to gaussian Cooper-pair fluctuations. Owing to their different physical character in Raman, we separate in the following discussion the two contributions.

## 4. Anomalous Raman spectra: The charge gaussian contribution

By suitably choosing the polarization of the incoming and outgoing photons in Raman scattering experiments, momentum-dependent vertices are introduced in the response, which select the regions in momentum space from where excitations are originated [29]. As a consequence, characteristic features arise in the Raman response with distinct doping and polarization dependencies which in turn allow to extract valuable informations about the excitations. This is the main issue of this work, where we will consider the $B_{2g}$ channel with a vertex $\gamma_{B_{2g}} = \sin k_x \sin k_y$ large along the diagonals of the Brillouin zone, and the $B_{1g}$ channel with a vertex $\gamma_{B_{1g}} = \cos k_x - \cos k_y$, which is large around the "hot" region near the $(\pm\pi, 0)$ and $(0, \pm\pi)$ points. In Ref. [30] it was found that Raman spectra display low-energy anomalous absorption in the $B_{2g}$ channel at low doping $x < 0.05$ and in the $B_{1g}$ channel at higher dopings. These low-energy features were attributed [21] to gaussian fluctuations of the charge density (quite similarly to the Cooper pair gaussian fluctuations in the Aslamazov-Larkin theory of paraconductivity). Based on symmetry arguments it was also shown that only charge CM could contribute with specific momentum structures, which agree with the ones inferred from neutron-scattering experiments [31]. Quite remarkably, the anomalous spectral features were fitted at various temperatures by simply adjusting the CM mass $m(x,T)$. This allowed us a straightforward determination of the T-dependence of $m$, which displayed the linear behavior expected for a quantum-critical CM crossing over below a temperature $T^*$ to a saturated nearly constant behavior typical of a state with "quenched" criticality with local-slow order (but without the long-range order, which would correspond to $m = 0$). This allowed to identify $T^*$ at two doping values, which (roughly) extrapolated to zero $[T^*(x_c) = 0]$ at a critical doping $x_c$ to be identified with the QCP doping[21,30]. These results were confirmed by a more recent systematic analysis [32] at several other doping values. The recent analysis of the LSCO results includes samples at low and moderate doping levels having anomalous scattering in both the $B_{2g}$ and $B_{1g}$ channels, respectively. This allows us to draw some conclusions: i) there is a crossover temperature $T^*$, clearly related to CO, which decreases upon increasing doping. Its doping dependence closely follows the doping dependence of the crossover temperature for the opening of the pseudogap. This allows us to clearly relate the latter one to CO; ii) this conclusion is further strengthened by the observation that the the electronic DOS starts to be substantially reduced in the background spectra (i.e., in spectral ranges completely separated by the anomalous features) below the same temperature $T^*$. This provides a completely independent determination of $T^*$, which is consistent with the $T^*$ obtained from $m(x,T)$; iii) the extrapolated $T^*$ vanishes around optimal doping at $0.16 < x_c < 0.19$, thereby indicating this range to be the location of the CO-QCP.

We also notice that the analysis of gaussian CO fluctuations in the $B_{1g}$ Raman spectra allows us to identify some key parameters of the CM in Eq. (1). In particular the mass $m$ and the "diffusivity" scale $\overline{\Omega}$ can be estimated by considering the low-energy side of the spectra. As we shall see in the next section, these quantities together with the high-energy cutoff $\Lambda$, determine the spectral function of the CO-CM, which can account for the overall shape of the $B_{2g}$ spectra.

## 5. Disentangling spin and charge fluctuations from $B_{1g}$ and $B_{2g}$ spectra

To analyze the whole spectra over a broader energy range, we need to consider physical processes where the CMs dress the fermionic QPs. We accordingly define a non-resummed Raman response $\tilde{\chi}_{S-V}$ from the first two diagrams of Fig. 1. The presence of impurities can be described introducing the memory function $M_{S-V} = i\Gamma - \omega\tilde{\chi}_{S-V}/W$, where $W$ is the optical weight and $\Gamma$ is the impurity scattering rate. The full Raman response function is then found as

$$\chi_{S-V} = \frac{W\omega}{\omega + M_{S-V}(\omega)}. \tag{2}$$

The S-V Raman response function of the corresponding CM can be written as in Eq.(2). The memory function can be cast in the perturbative form [28]

$$Im\, M_{S-V}(\omega) = \frac{g_\alpha^2}{\omega}\int_0^\infty dz\, [\alpha^2 F(\omega)]\, \Big[2\omega \coth\left(\frac{z}{2T}\right) - (z+\omega)\coth\left(\frac{z+\omega}{2T}\right) + (z-\omega)\coth\left(\frac{z-\omega}{2T}\right)\Big] \tag{3}$$

where T is the temperature and the CM spectral strength is

$$\alpha^2 F(\omega) = \arctan\left(\frac{\Lambda\overline{\Omega} - \omega^2}{\overline{\Omega}\omega}\right) - \arctan\left(\frac{m\overline{\Omega} - \omega^2}{\overline{\Omega}\omega}\right) \tag{4}$$

The real part of $M_{S-V}$ is found by Kramers-Kronig transformation.

We are now in a position to make a simple working hypotesis: We assume that the CM's (both spin and charge) provide the interelectronic scattering needed to account for the whole Raman spectra over the entire frequency range up to $\omega = 8000$ cm$^{-1}$. The important step further is to recognize that the momentum dependence of the CO and spin CM's is such that their *leading-order* contributions via the diagrams S and V of Fig. 1, act separately in the different channels. Specifically one can show that the (leading-order) contribution of the spin-CM only acts in the $B_{1g}$ channel, while it is cancelled in the $B_{2g}$. The reverse is true for the CO-CM. This leading-order separation allows to retrace back the difference in the spectra to differences of the CM producing the scattering in each channel. Specifically, large values of $\overline{\Omega}$ results in diffusive-like modes as shown in the inset of Fig. 2(b), while smaller values of $\overline{\Omega}$ give rise to more propagating modes with the square-like spectrum typical of a marginal Fermi-liquid displayed in the inset of Fig. 2(c). We find it remarkable that the generic quantum-critical form of the CM propagators in Eq. (1) can be tuned to display either the character of a diffusive critical mode or that of a marginal-Fermi-liquid mediator.

Since we aim to keep the treatment as simple as possible and to carry out analytical calculations as far as possible, we choose to insert free quasiparticles in the S-V diagrams thereby disregarding the pseudogap effects on the fermions.

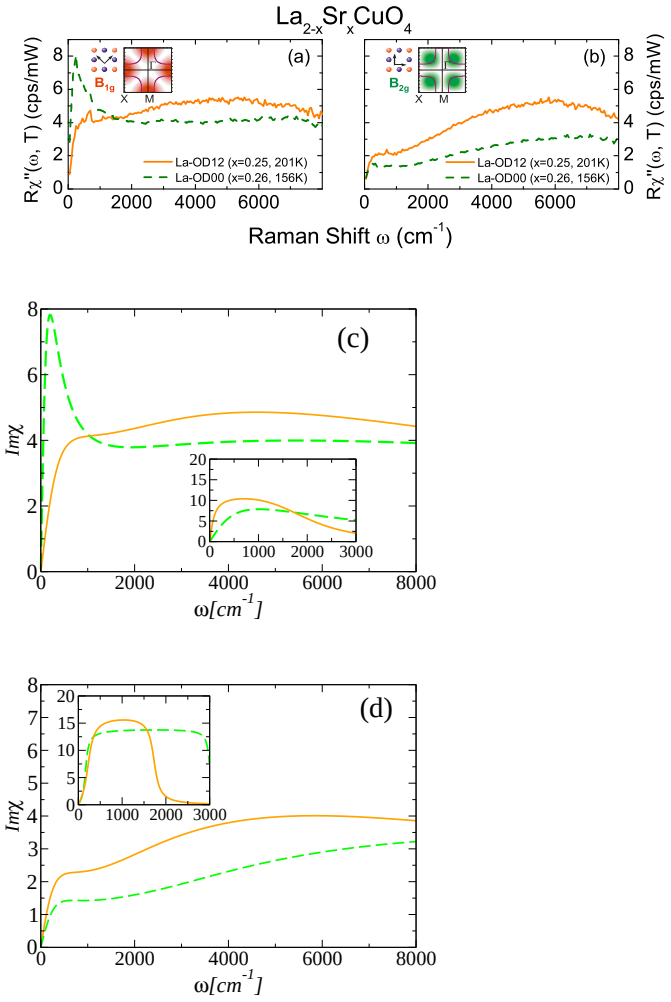


Fig. 2. Raman spectra in the $B_{1g}$ channel (a) and $B_{2g}$ channel (b) for a LSCO sample at $x = 0.25$ (solid curves) and $x = 0.26$ (dashed curves). (c) $B_{1g}$ Raman spectra calculated from spin CMs with the $\alpha^2 F$ displayed in the inset with $m_s = 80$, $\overline{\Omega}_s = 10^5$, $\Lambda_s = 2000$, and $g_s^2 = 12.1$ (solid curve) and $m_s = 500$, $\overline{\Omega}_s = 5 \cdot 10^5$, $\Lambda_s = 2000$, and $g_s^2 = 7.3$ (dashed curve) (all energy units are in cm$^{-1}$). (d) $B_{2g}$ Raman spectra calculated from CO CMs with the $\alpha^2 F$ displayed in the inset with $m_c = 300$, $\overline{\Omega}_c = 200$, $\Lambda_c = 15000$, and $g_c^2 = 5.5$ (solid curve) and $m_c = 300$, $\overline{\Omega}_c = 100$, and $\Lambda_c = 90000$ and $g_c^2 = 4.5$ (dashed curve) (all energy units are in cm$^{-1}$).

This is obviously justified only at sufficiently large dopings. This is why we consider the two ($B_{1g}$ and $B_{2g}$) spectra of two overdoped LSCO samples [32] reported in Figs. 2(a) and 2(b).

The most obvious changes with doping are observed in the $B_{1g}$ spectra (Fig. 2(a)). While there is a well defined peak in the range 200 to 500 cm$^{-1}$ followed by a flat part up to 8000 cm$^{-1}$ in the non-superconducting sample ($x = 0.26$; dashed line), the low-energy peak is completely absent at $x = 0.25$ ($T_c \approx 10K$; full line), and only a hump below 100 cm$^{-1}$ is left. The differences are more more subtle in $B_{2g}$ symmetry (Fig. 2 (b)). As a general feature there is a hump at approximately 500 cm$^{-1}$. At $x = 0.25$ (full line) the subsequent increase occurs in a range of 3000 cm$^{-1}$ 1ending in a broad maximum at 5000 cm$^{-1}$. At $x = 0.26$ (dashes)

the increase is very smooth and there is no maximum any more in the observed range.

We then notice that even at fixed doping the spectra look qualitatively different in the two channels. In particular, for the $x = 0.25$ sample, while the $B_{1g}$ spectrum has the rounded shape of a hump plus a (slightly higher) hump, the $B_{2g}$ spectrum looks like a flattish step followed by a substantially (nearly a factor two) higher hump. This behavior is also observed at lower doping levels [32]. Starting from different shapes of the spin and charge CMs (see full curves in the insets) we reproduce quantitatively the spectra in the two channels. Of course the precise fitting of the spectra would require the adjustment of many parameters. The resummed spectra derived from Eq. (2) depend on the optical weight $W$, on the elastic scattering from impurities $\Gamma$ as well as on the parameters of the CMs. To extract qualitative informations on these latters we choose to keep $W$ and $\Gamma$ fixed trying to reproduce the semiquantitative behavior of the spectra by only adjusting the CM parameters. Specifically we find that the $B_{1g}$ spectrum arises from (spin) modes with a substantially diffusive form ($\overline{\Omega}_s \approx 5 \cdot 10^4$ cm$^{-1}$, $m_s \approx 80$ cm$^{-1}$) with a rapid rise of the spectrum reaching a broad maximum around 500-700 cm$^{-1}$. The spin mode then "dies" above a frequency of about 2000 cm$^{-1}$. On the other hand, the $B_{2g}$ spectrum of the $x = 0.25$ sample acquires the step+hump shape if a (charge) CM is chosen with a markedly propagating character [$\overline{\Omega}_c \approx 10^2$ cm$^{-1}$) and $m_s \approx 500$ cm$^{-1}$]. The low-energy weight of this mode only arises from its small diffusivity and then substantially rises only around 300 cm$^{-1}$. Also this mode no longer exists above a typical frequency of the order of 2000 cm$^{-1}$.

Upon slightly increasing the doping to $x = 0.26$ the $B_{2g}$ (charge-related) spectrum changes little in shape and is simply reduced in intensity. Also the related collective mode stays propagating and it is just moderately reduced in intensity. To account for the data one only needs to consider a broader spectral range extending up to 3000 cm$^{-1}$. On the contrary, the spin-related $B_{1g}$ spectrum changes remarkably in shape: It has a narrow Drude-like form at low frequency and then flattens and stays nearly constant up to high frequencies. This behavior is recovered in the theoretical spectrum by choosing an even more strongly damped mode ($\overline{\Omega}_s \approx 10^5$ ) (which reduces the overall height of the spectrum) and by further increasing the mass $m_s = 500$ cm$^{-1}$. This increase lowers the spectral weight at low frequency thereby reducing the scattering due to this mode. In this way the narrow Drude-like peak is obtained. Then, as soon as the frequency increses, the broad spectrum of the mode enters into play producing the flattening of the $B_{1g}$ spectrum.

## 6. A brief analysis of optics

The above analysis of Raman spectra exploited the Raman form factors to identify the role of spin and charge CMs in the various channels. This distinction is no longer possible in optical conductivity, where all the different CMs equally contribute to the spectra. Another remarkable difference is that optical spectra strongly depend on the momentum-charge conservation laws, which may introduce additional energy scales related to the dissipation mechanisms [27]. As a consequence of the conservation laws, all the contributions from the diagrams of Fig. 1 are tightly related and implement conspicuous concellations in the case of nearly clean systems. Here we will instead neglect these effects assuming that the momentum conservation is substantially violated both from static, Umklapp, and dynamical dissipation mechanisms. In this case the S-V and AL contributions in the current-current response no longer display severe cancellations and one can obtain a semiquantitative estimate of optical spectra from the S-V contributions only. This is what we carry out in this section by replacing the Raman response $\tilde{\chi}_{S-V}$ entering the memeory function with the current-current response $\tilde{\chi}_{jj}$ thereby obtaining the optical memory function $M_{opt} = i\Gamma - \omega\tilde{\chi}_{jj}/W$. We then are in the position to qualitatively compare the contribution of CO *and* spin CM (they act on equal footing in optics) to the optical memory function recently obtained in experiments [10]. For an illustrative purpose we calculate the optical memory function by simply adding the effects of the CO and spin CMs. The result is reported in Fig. 3, where the memory function of a spin CM (black curve) with diffusive character and moderate mass is displayed together with the memory function of a CO-CM with smaller mass and a more propagating character. Clearly the resulting total memory function (red curve) is similar to the ome reported in Fig. 1 of Ref. [10] for an optimally doped $HgBa_2CuO_{4=\delta}$ sample in the normal state well above $T_c$. The purpose here is not to carry out a detailed quantitative comparison, but simply to show that our scheme based on the coexistance of spin and CO modes may account for optical data as well. We also notice in passing that our scenario in principle is not in contradiction with the one presented in Ref. [10], where two markedly distinct features were deduced in the bosonic spectra. In our case the low-energy bosonic part of the spectrum would correspond to the more propagating CO modes, while the broader part of the bosonic spectrum at higher energy should be identified with the spin diffusive modes.

## 7. Discussion and conclusions

The results reported in the previous sections are relevant for several reasons. First of all, the very fact that the spectra in the various channels are different and can be accounted for by scattering due to CMs with different momentum structures, is an indication that the physics of the cuprates is not ruled by zero momentum modes or by local nearly structureless modes. Then one is led to conclude that i) retarded interactions with momentum structure at

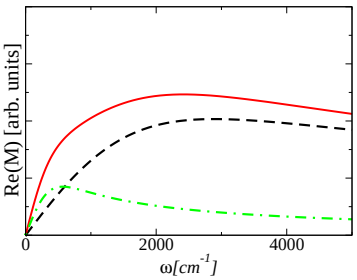


Fig. 3. Optical memory function (arbitrary units) obtained from the summed effect of a CO CM with $m_c = 30$, $\overline{\Omega}_c = 20$, and $\Lambda_c = 2000$ (dot-dashed line) and a spin CM with $m_s = 400$, $\overline{\Omega}_s = 2000$, and $\Lambda_s = 2000$ (dashed line). The overall coupling factor are $g_c^2 = 5$ and $g_s^2 = 1$ (all energy units in $\mathrm{cm}^{-1}$)

finite wavevectors are at work. ii) The temperature dependence of (the mass of) these modes is relevant to account for the temperature dependence of the low-energy anomalous features. Moreover if one keeps the mass of the modes (i.e. their typical low energy scale) temperature independent, the resulting spectra depend too strongly from temperature (even at large frequencies) in comparison to the experimental Raman spectra. This arises because the bosonic caracter of the modes introduces Bose distribution functions, which substantially depend on temperature [28,33]. iii) To recover the (near) temperature independence of the observed spectra at high frequency one has to keep the precise temperature dependence of the mass [33]. We also found that both charge and spin modes contribute to scattering allover the frequency range. Our leading-order symmetry arguments then allowed us to identify the contribution of each mode in the different channels. However, one should also keep in mind that the pretemption to account for the shape of the spectra keeping separate the spin and charge contribution looses its validity at energies as high as several thousends of $\mathrm{cm}^{-1}$. The symmetry arguments based on the critical structure (i.e. strongly momentum dependent at low energies) are no longer justified at such high energy and only provide rough indications. Moreover, not only the symmetry arguments to distinguish spin and charge contribution become unreliable, but also the physical distinction between these modes is questionable: Indeed a strong mixing of the spin and charge degrees of freedon is observed in LSCO above this energy scale [34]. In the light of all these consideration one can then understand why above 4000 $\mathrm{cm}^{-1}$ the spectra in both channels become quite similar signaling that the distinction between spin and CO CM breaks down at high energy.

Nevertheless we find remarkable that the differences in the spectra are understood in terms of scattering due to CMs with different characteristics. Namely, the spin modes are strongly overdamped and rapidly loose intensity upon increasing doping. This behavior is also clearly observed in inelastic neutron scattering [22,23,24]. In particular, we find that the strong reduction (by nearly a factor of two in the spin DOS) in going from $x = 0.25$ to $x = 0.26$ is in qualitative agreement with a similar reduction observed in the neutron spectra of Ref. [24] in passing from $x = 0.25$ to $x = 0.27$. We also find it quite reasonable that in the same doping range, the CO-CMs are more stable upon doping and are more propagating (i.e. less damped). This is what is expected for critical modes which are much closer to their QCP (which we locate around $x = 0.18$ from the low-energy anomalies).

## References


[1] P.W. Anderson, Science **235**, 1196 (1987).
[2] P. W. Anderson, *The theory of high $T_C$ superconductivity in the High-$T_c$ cuprates*, Princetn University Press, Princeton 1997.
[3] V.J. Emery and S.A. Kivelson, Physica (Amsterdam) **209C**, 597 (1993).
[4] P.W. Anderson, Science **316**, 1705 (2007).
[5] C. M. Varma, Phys. Rev. Lett. **75**, 898 (1995); Phys. Rev. B. **55**, 14554 (1997), and references therein.
[6] C. Castellani, C. Di Castro, and M. Grilli, Phys. Rev. Lett. **75**, 4650 (1995).
[7] A. Abanov, *et al.*, Adv. Phys. **52**, 119 (2003), and references therein.
[8] T. A. Maier, D. Poilblanc, and D. J. Scalapino, arXiv:0801.4506
[9] S.V. Dordevic et al., Phys. Rev. B 71, 104529 (2005) and refs. therein.
[10] E. van Heumen, et al., arXiv:0807.1730v1.
[11] M. Capone *et al.*, Phys. Rev. Lett. **92**, 106401 (2004)
[12] W. Metzner, D. Rohe, and S. Andergassen, Phys. Rev. Lett. **91**, 066402 (2003).
[13] For an early review on evidences of CO-QCP near optimal doping see, e.g., C. Castellani, C. Di Castro, and M. Grilli, J. of Phys. and Chem. of Solids **59**, 1694 (1998).
[14] J. Zaanen and O. Gunnarsson, Phys. Rev. B**40**, 7391 (1989).
[15] R. Raimondi, *et al.*, Phys.Rev. B **47**, 3331 (1993)
[16] U. Löw, *et al.*, Phys. Rev. Lett. **72**, 1918 (1994).
[17] A. Perali, C. Castellani, C. Di Castro, and M. Grilli, Phys. Rev. B **54**, 16216 (1996)
[18] S. Andergassen, S. Caprara, C. Di Castro, and M. Grilli, Phys. Rev. Lett.**87**, 056401 (2001).
[19] G. Seibold and M. Grilli, Phys. Rev. B **63**, 224505 (2001)
[20] S. Caprara, M. Grilli, C. Di Castro, and T. Enss, Phys. Rev. B **75**, 140505 (2007)
[21] S. Caprara, C. Di Castro, M. Grilli, and D. Suppa, Phys. Rev. Lett. **95**, 117004 (2005).
[22] S. Wakimoto, *et al.* Phys. Rev. Lett. **92**, 217004 (2004)
[23] O. J. Lipscombe, *et al.* Phys. Rev. Lett. **99**, 067002 (2007)
[24] S. Wakimoto, *et al.* Phys. Rev. Lett. **98**, 247003 (2007)
[25] M. Enoki, S. Fujita, and K. Yamada, arXiv:0804.2723
[26] J. A. Hertz, Phys. Rev. B **14**, 1165 (1976).
[27] S. Caprara, M. Grilli, C. Di Castro, and T. Enss, Phys. Rev. B, **75**, 140505(R) (2007).
[28] M. R. Norman and A. V. Chubukov, Phys. Rev. B **73** (2006) 140501(R).
[29] See, e.g., T. P. Devereaux, A. Virosztek, and A. Zawadowski, Phys. Rev. B **51**, 505 (1995).
[30] L. Tassini *et al.*, Phys. Rev. Lett. **95**, 117002 (2005)
[31] K. Yamada, *et al.*, Phys. Rev. B **57**, 6165 (1998).
[32] B. Muschler, Diploma Thesis, Technische Universität München, unpublished (2007).
[33] S. Caprara, M. Grilli, C. Di Castro, and T. Enss, to appear in J. of Magn. Mag. Mat., arXiv:0805.4291
[34] M. Grilli, G. Seibold, J. Lorenzana, and A. Di Ciolo, unpublished